Supporting Information for Hydrodynamic-Induced Conformational Transitions of Charged Macromolecules Dictate Anomalous Electroosmotic Flow

Kuo Chen[1] and Minglun Li[2,3,*]

[1] *Department of Polymer Science and Engineering, University of Massachusetts, Amherst, Massachusetts 01003, United States*

[2] *State Key Laboratory of Polymer Science and Technology, Changchun Institute of Applied Chemistry, Chinese Academy of Sciences, Changchun 130022, P. R. China*

[3] *School of Applied Chemistry and Engineering, University of Science and Technology of China, Hefei 230026, P. R. China*

(Dated: March 19, 2026)

I. DETAILED SIMULATION PROTOCOLS AND PARAMETERS

A. Interparticle Potentials

Our explicit-solvent models consist of a single charged macromolecule (either a positively or negatively charged chain) with its neutralizing counterions, solvent beads, added ions, and the discrete wall beads. The macromolecule with a degree of polymerization $N = 50$ was placed in a solid-state nanopore with a fixed radius R aligned along the x-axis. The macromolecule and free ions are treated as charged beads of the same diameter, $\sigma = 0.70$ nm serves as the characteristic length unit of the study. Each monomer carries one negative (e)/positive ($-e$) charge, with e being the elementary charge. The counterion is a monovalent ion with a charge opposite to that of the monomer.

To maintain strict steric hindrance while ensuring computational efficiency, the short-range repulsive interactions for solute-solute and solute-wall particles sterics were described by the purely repulsive Weeks-Chandler-Andersen (WCA) potential:

$$U_{\mathrm{WCA}}(r_{ij}) = \begin{cases} 4\varepsilon \left[\left(\frac{\sigma}{r_{ij}}\right)^{12} - \left(\frac{\sigma}{r_{ij}}\right)^{6} \right] + \varepsilon, & r_{ij} \le r_0 \\ 0 \qquad\qquad , & r_{ij} > r_0 \end{cases} \tag{S1}$$

where r_{ij} is the inter-particle distance. $\varepsilon = k_{\mathrm{B}}T$ is the energy unit with k_{B} being the Boltzmann constant and $T = 300$ K the absolute temperature. $r_0 = 2^{1/6}\sigma$ is the cutoff distance to avoid bead–bead overlap and to simulate a good solvent condition.

Connectivity between adjacent monomers along the macromolecule backbone was maintained by the finitely extensible nonlinear elastic (FENE) potential to prevent nonphysical bond crossing:

$$U_{\mathrm{bond}}(r) = -\frac{1}{2} K r_{\mathrm{bond}}^2 \ln\left[1 - \left(\frac{r_{ij}}{r_{\mathrm{bond}}}\right)^2\right] \tag{S2}$$

Following classical polymer physics parameterizations, the spring constant was set to $K = 30\varepsilon/\sigma^2$ and the maximum bond extension to $r_{\mathrm{bond}} = 1.5\sigma$. As fully flexible chains are modeled in our study, additional angle and dihedral potentials were not included.

Electrostatic interactions between charged particles were evaluated using the Coulomb potential:

$$U_{\mathrm{ele}}(r_{ij}) = k_{\mathrm{B}}T l_{\mathrm{B}} \frac{z_i z_j}{r_{ij}} \tag{S3}$$

where z_i and z_j are the valences of the particles. l_{B} represents the Bjerrum length characterizing the dielectric properties of the medium. For aqueous solution, $l_{\mathrm{B}} = \frac{e^2}{4\pi\epsilon_0\epsilon_{\mathrm{w}}k_{\mathrm{B}}T} \approx 0.7\mathrm{nm} = \sigma$ with ϵ_0 and ϵ_{w} being the vacuum permittivity and relative dielectric constant of water, respectively. Long-range electrostatic interactions beyond the cutoff radius were efficiently resolved using the particle-particle particle-mesh (PPPM) algorithm with a target accuracy of 10^{-5}.[1, 2] The simulations were under three-dimensional periodic boundary conditions. To eliminate spurious

* mlli@ciac.ac.cn

transverse electrostatic couplings between adjacent periodic images, the simulation box dimensions in the y and z directions were expanded to ten times the channel diameter ($10R$), creating a sufficient vacuum gap. Meanwhile, the axial box length in the x-direction was set significantly larger than the extended polymer chain dimension to prevent artificial self-interactions, with specific box lengths for different systems detailed in Table S1.

TABLE S1. The Simulation System Parameters

R/σ	$c_s\ \sigma^3$	n_+ [a]	n_- [b]	L_x/σ [c]	L_y/σ [d]	L_z/σ [e]
1.5	0.10	270	23	200	10	10
2.7	0.10	840	301	241	27	27
3.0	0.10	816	329	196	30	30
3.3	0.10	789	349	161	33	33
4.0	0.04	468	104	110	40	40
4.0	0.10	753	390	110	40	40
5.0	0.10	733	436	72	50	50
6.0	0.04	350	108	49	30	30
6.0	0.10	649	451	49	30	30
7.0	0.10	677	468	36	35	35

[a] The number of free cations in the system.
[b] The number of free anions in the system.
[c] The length of the simulation box in the x-direction.
[d] The length of the simulation box in the y-direction.
[e] The length of the simulation box in the z-direction.

B. Dissipative Particle Dynamics (DPD) Framework

The macromolecule chain and counterions are explicitly solvated using the DPD framework. Each DPD bead represents three water molecules, maintaining a number density of $\rho_s = 3\sigma^{-3}$. Consistent with established DPD methodologies, the pairwise interactions between particles are governed by three distinct forces:

$$\mathbf{F}_{ij}^{C} = A_{ij}(1 - \frac{r_{ij}}{r_c})\hat{\mathbf{r}}_{ij} \tag{S4}$$

$$\mathbf{F}_{ij}^{D} = -\gamma\omega^{D}(r_{ij})(\mathbf{v}_{ij} \cdot \hat{\mathbf{r}}_{ij})\hat{\mathbf{r}}_{ij} \tag{S5}$$

$$\mathbf{F}_{ij}^{R} = \sqrt{2\gamma k_B T}\omega^{R}(r_{ij})\frac{\zeta_{ij}}{\sqrt{\Delta t}}\hat{\mathbf{r}}_{ij} \tag{S6}$$

$\mathbf{F}_{ij}^{C}$, $\mathbf{F}_{ij}^{D}$, and $\mathbf{F}_{ij}^{R}$ denote the conservative (soft repulsive), dissipative, and random forces, respectively. The latter two act collectively as a momentum-conserving thermostat. A_{ij} specifies the maximum repulsion strength, the solvent-solvent interaction parameters are configured as $A_{ij} = 78k_BT$ to reproduce the macroscopic compressibility of water at room temperature. $\hat{\mathbf{r}}_{ij}$ is the unit interparticle vector, and $r_c = \sigma$ represents the universal cutoff radius. $\mathbf{v}_{ij} = \mathbf{v}_i - \mathbf{v}_j$ is the relative velocity, and $\hat{\mathbf{r}}_{ij}$ is the unit inter-particle vector. γ is the friction coefficient, and $\gamma = 4.5k_BT\tau\sigma^{-2}$ for the solvent and τ is the time scale. The standard weight functions were chosen as $\omega^{D}(r_{ij}) = [\omega^{R}(r_{ij})]^2 = (1 - \frac{r_{ij}}{r_c})^2$. Solute-solvent interactions are mediated exclusively via the DPD thermostat; by setting the cross-interaction friction to $\gamma_s = 5\gamma$ with $r_c = \sigma$.

The entire fluidic system is confined within a nanopore. The DPD solvent particles interact with the smooth confining surfaces via the purely repulsive WCA potential (Eq. S1). These effective boundary surfaces are positioned at $r_{wall} = \pm(R/2 + r_c)$,[3] while immobile wall particles are explicitly placed at $\pm R/2$ with a 2D number density of $r_{im} = \rho_s r_c$. To regulate the wall–fluid friction, an additional dissipative and random force is applied between

TABLE S2. Electric Field and Péclet Number

Electric Field (E)	0.0027	0.0054	0.027	0.0539	0.0809	0.1348	0.2696	0.5392	1.0784	2.1568	3.2352	4
Pe	0.18	0.36	1.79	3.58	5.36	8.94	17.88	35.76	71.52	143.03	214.55	268.18

fluid particles and the wall within a cutoff distance of σ, utilizing an effective friction coefficient of $\gamma_{\rm ns} = 4\gamma$. The factor "4" used in this work provides a moderate wall–fluid coupling strength that effectively suppresses excessive boundary slip without inducing unphysical over-damping of the near-wall dynamics.[4] The particles of the nanopore wall are uniformly assigned negative surface charges, with a surface charge density of $-0.132e/\sigma^2$. This corresponds to $0.05\mathrm{C/m}^2$, a typical value for solid-state nanopores.[5]

C. Boundary Conditions and Simulation Protocol

A uniform external electric field E was applied along the axial x-direction to simultaneously drive the electrophoresis of the macromolecule and the electro-osmosis of the counterion-rich fluid. We systematically investigated a broad spectrum of reduced electric field strengths ranging from $E = 0.0027$ to 4.0. Specifically, $E = 0.1348$ corresponds to the typical electric field strength used in experiments, e.g., a transmembrane potential of 120mV across a solid-state nanopore (15 nm thick, R =5 nm) with bulk solution concentration $c_{\rm s} = 0.5$ M.[6] To quantify the relative magnitude of the external electrical work compared to thermal fluctuations, we define a dimensionless reduced electric field, serving as an electrical Péclet number:

$$Pe = \frac{EN|q_{\rm eff}|R_{\rm g}}{k_{\rm B}T} \tag{S7}$$

$q_{\rm eff} = -0.24e$ and $R_{\rm g} = 5.62\sigma$ represent the effective charge and radius of gyration per monomer in bulk solution, respectively. $q_{\rm eff}$ was determined by averaging the net charge within the Debye radius of each monomer during simulation. Since $q_{\rm eff}$ and $R_{\rm g}$ remain stable across the investigated electric field range (varying only at extreme intensities as shown in Fig. S1), bulk values are used to calculate Pe. The relationship between E and Pe is shown in Table S2.

To systematically investigate confinement effects comparing with the size of the macromolecule (radius of gyration $R_{\rm g}$) from the strongly squeezed ($R \ll R_{\rm g}$) to the weakly confined ($R > R_{\rm g}$) regimes, the pore radius R was varied from 1.5σ to 7σ. To maintain a consistent Debye screening length ($\lambda_{\rm D}$) across all R, the total ion number density was fixed to match the reservoir salt concentration ($c_+ + c_- = 2c_{\rm s}$). Global electroneutrality was simultaneously enforced by offsetting the surface charge via the ion concentration difference ($c_+ - c_- = \frac{2|\nu|}{eR}$), where c_+, c_-, and $c_{\rm s}$ are the number densities of cations, anions, and the reservoir salt, respectively. This initialization strategy prevents the artificial over-screening caused by unbounded counterion addition, ensuring the pore ion concentrations remain quantitatively consistent with continuum finite element method calculations at the same $c_{\rm s}$.[6]

The pairwise nature of the DPD forces rigorously satisfies Newton's third law. The equations of motion are integrated using the Velocity-Verlet algorithm with a time step of $\Delta t = 0.005\tau$. Prior to the application of the electric field and data collection, the system undergoes a thorough relaxation phase to ensure thermal equilibrium for 1×10^6. Production runs for sampling physical properties span 5×10^6 time steps. All molecular dynamics trajectories are generated utilizing the Large-scale Atomic/Molecular Massively Parallel Simulator (LAMMPS).[7]

D. Derivation of the Fluid Velocity Profile

The local net charge density of the fluid is extracted from the DPD simulations by summing the concentration contributions of all mobile ion species:

$$\rho_{\rm net}(\mathbf{r}) = e c_{\rm net}(\mathbf{r}) \tag{S8}$$

$c_{\rm net}(\mathbf{r}) = c_+(\mathbf{r}) - c_-(\mathbf{r}) \pm c_{\rm counter}(\mathbf{r})$, where the sign of the counterion term depends on the macromolecule charge, taking "+ "for negatively charged macromolecule and "−" for positively charged one.

The time dependence of the velocity of fluid flow ($\boldsymbol{v}_{\rm EOF}$) is obtained by the Navier–Stokes equation:

$$m_0 \frac{\partial \boldsymbol{v}_{\rm EOF}(\mathbf{r},t)}{\partial t} + \boldsymbol{v}_{\rm EOF} \cdot \nabla \boldsymbol{v}_{\rm EOF}(\mathbf{r},t) - \eta \nabla^2 \boldsymbol{v}_{\rm EOF}(\mathbf{r},t) + \nabla p(\mathbf{r},t) = \boldsymbol{F}(\mathbf{r},t) \tag{S9}$$

where $p(\mathbf{r},t)$ is the local pressure field, m_0 is the mass density of the fluid, and η is the shear viscosity of the fluid, $\eta = 8.904\times10^{-4}$ Pa·s for water. In this work, we use the number of $\eta = 1.65\varepsilon\tau\sigma^{-3}$ for reduced unit for the best fitting of the spatial velocity distribution of fluid particles (Fig. S2). $\boldsymbol{F}(\mathbf{r},t)$ is an external force, and $\boldsymbol{F}(\mathbf{r}) = \rho_{\text{net}}(\mathbf{r})\boldsymbol{E}(\mathbf{r})$ in this work.

Assuming a fully developed, steady-state creeping flow in a uniform channel, the inertial terms and the axial pressure gradient vanish.[8] This yields the simplified Navier–Stokes equation for the creeping flow:

$$-\eta\nabla^2\boldsymbol{v}_{\text{EOF}}(\mathbf{r}) = \rho_{\text{net}}(\mathbf{r})\boldsymbol{E}(\mathbf{r}) \tag{S10}$$

II. ADDITIONAL FIGURES

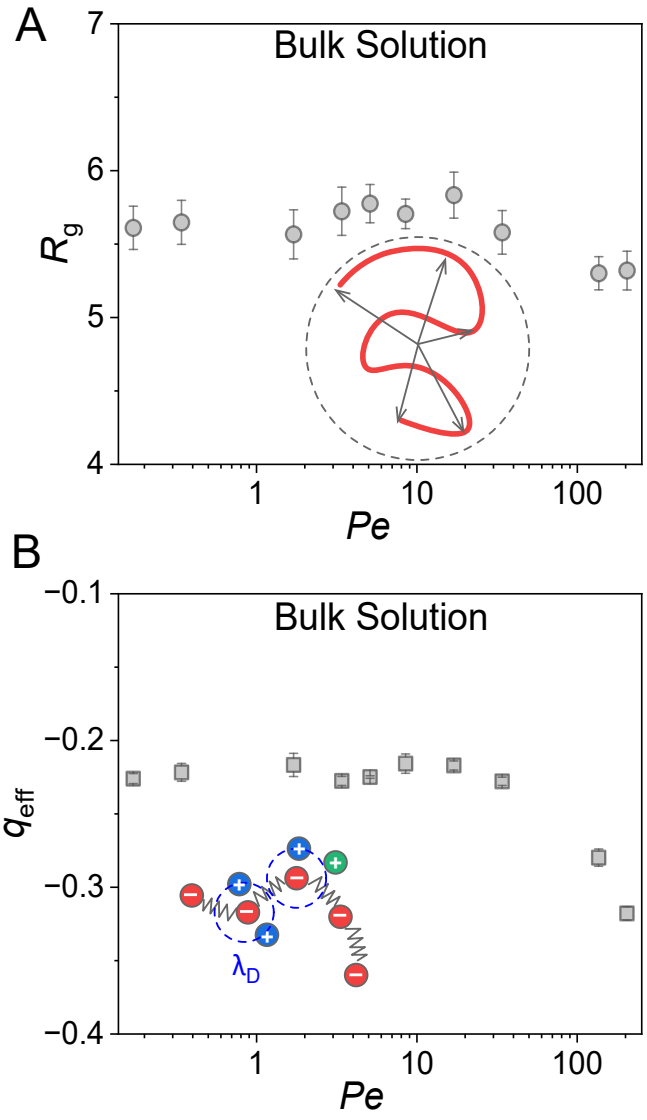

FIG. S1. Polymer properties in bulk solution. (A) Radius of gyration (R_g) versus Péclet number (Pe). The inset schematically illustrates R_g. (B) Effective charge (q_{eff}) versus Pe. The inset depicts the bead-spring macromolecule model and the Debye screening length (λ_D). The value of q_{eff} is calculated by summing all charges within λ_D around each monomer.

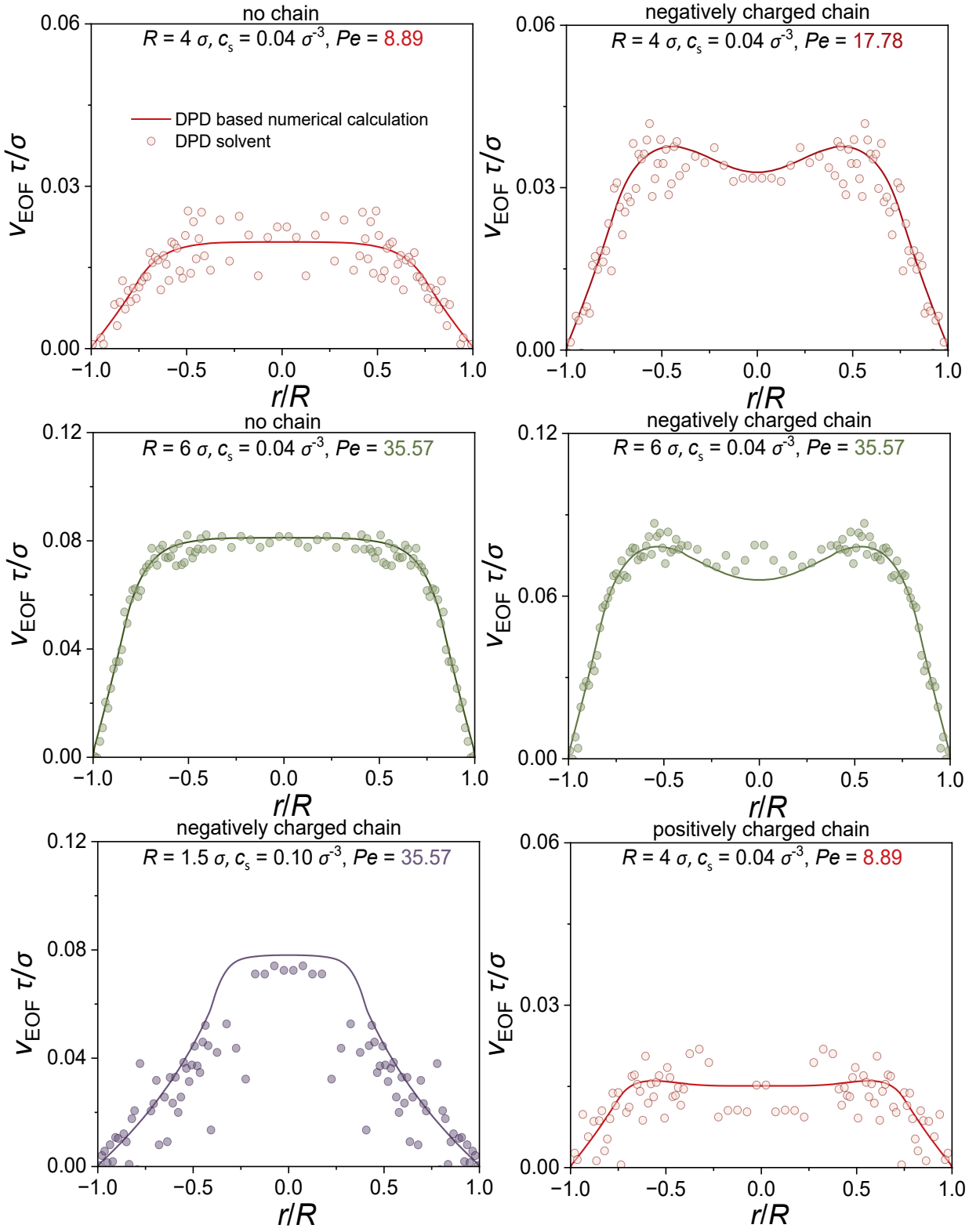

FIG. S2. EOF velocity profiles (v_{EOF}) along the radial direction (r/R) of the nanopore. The open circles represent the velocity distributions obtained directly from the DPD simulated solvent particles, while the solid lines denote the theoretical predictions derived from DPD-based numerical calculations. The subplots illustrate the effects of varying pore radii (R), salt concentrations (c_{s}), Péclet numbers (Pe), and the presence/type of a macromolecule chain (no chain, negatively charged chain, or positively charged chain) within the pore.

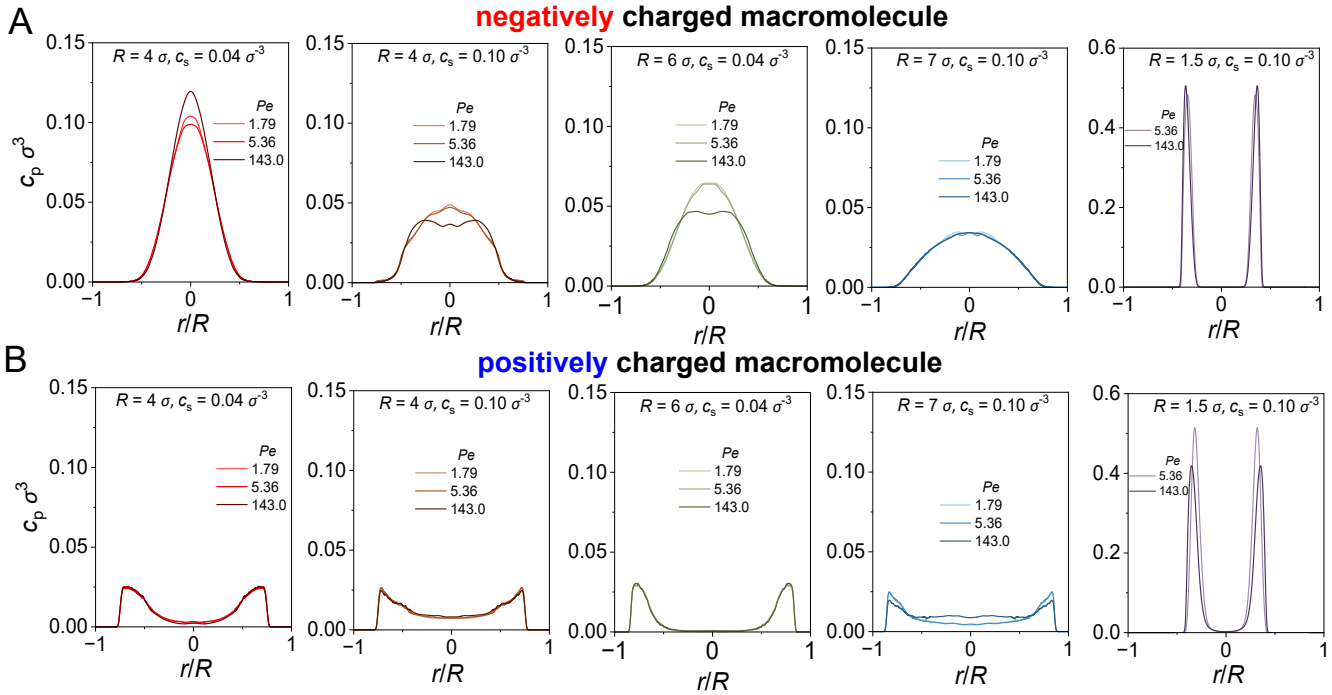

FIG. S3. Local charged macromolecule density (c_{p}) along the radial direction (r/R) of the nanopore.

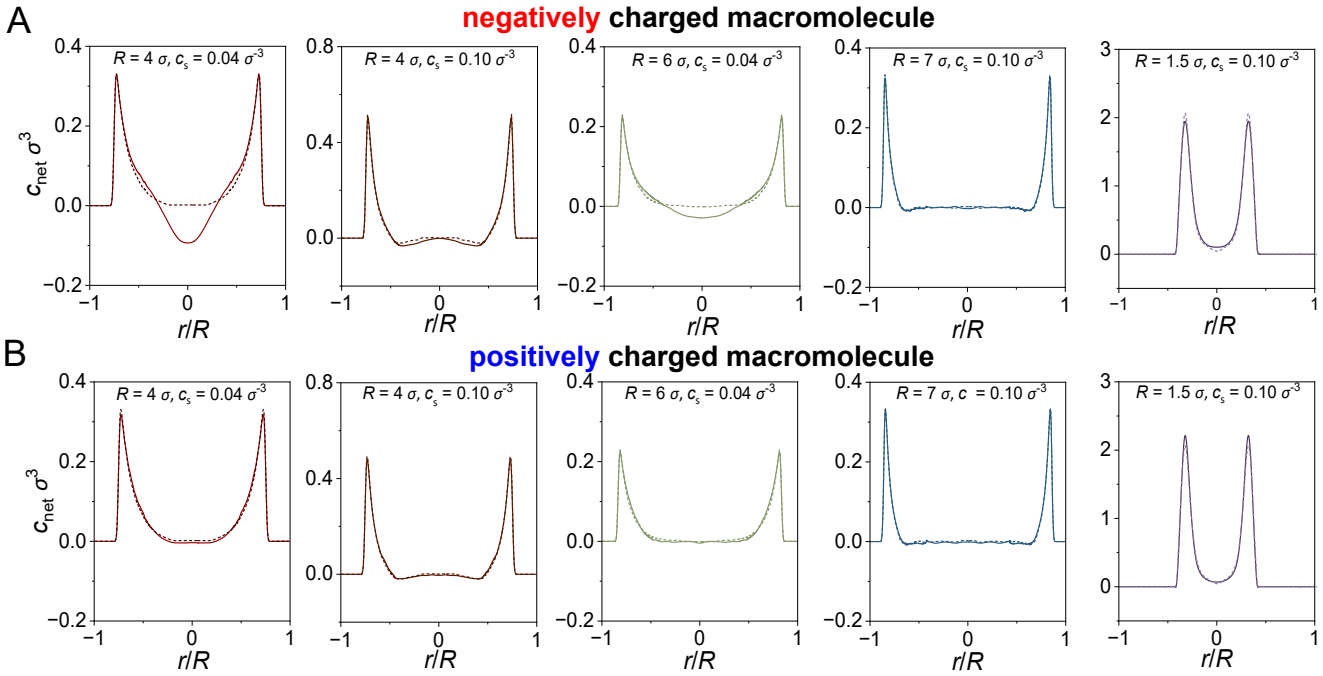

FIG. S4. Local net charge density (c_{net}) along the radial direction (r/R) of the nanopore.

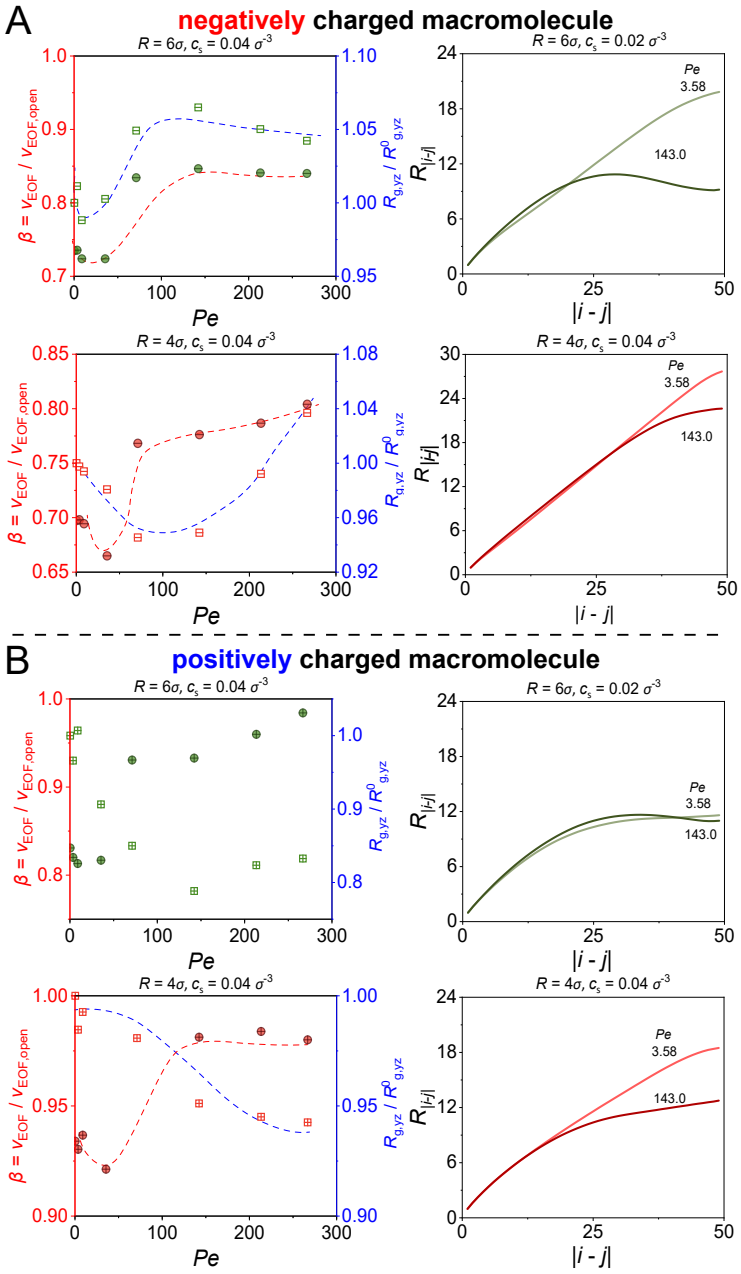

FIG. S5. Normalized centerline EOF velocity ($v_{\mathrm{EOF}}/v_{\mathrm{EOF,open}}$) versus normalized cross-sectional radius of gyration ($R_{\mathrm{g},yz}/R^0_{\mathrm{g},yz}$), alongside corresponding internal monomer distances ($R_{|i-j|}$) for (A) negatively and (B) positively charged macromolecules.

References

[1] J. W. Eastwood, R. W. Hockney, and D. Lawrence, P3M3DP-the three-dimensional periodic particle-particle/particle-mesh program, Comput. Phys. Commun. **19**, 215 (1980).

[2] B. A. Luty and W. F. van Gunsteren, Calculating electrostatic interactions using the particle- particle particle- mesh method with nonperiodic long-range interactions, J. Phys. Chem. **100**, 2581 (1996).

[3] T. Curk, Dissipative particle dynamics for coarse-grained models, J. Chem. Phys. **160** (2024).

[4] X. Liu, Z. Li, A. Yaroshchuk, W. Zhang, Y. Zhao, Q. Wang, A. S. Abd-El-Aziz, and C. Zhao, Polymer chain conformation triggers electro-osmotic flow in uncharged nanochannels, Macromolecules **58**, 13491 (2025).

[5] Y. Lee and M. Muthukumar, Charge symmetry breaking in neutral polyzwitterions, Nat. Commun. **16**, 3507 (2025).

[6] M. Li and M. Muthukumar, Electro-osmotic flow in nanoconfinement: Solid-state and protein nanopores, J. Chem. Phys. **160** (2024).

[7] A. P. Thompson, H. M. Aktulga, R. Berger, D. S. Bolintineanu, W. M. Brown, P. S. Crozier, P. J. In't Veld, A. Kohlmeyer, S. G. Moore, T. D. Nguyen, *et al.*, Lammps-a flexible simulation tool for particle-based materials modeling at the atomic, meso, and continuum scales, Comput. Phys. Commun. **271**, 108171 (2022).

[8] L. D. Landau and E. M. Lifshitz, *Fluid Mechanics: Landau and Lifshitz: Course of Theoretical Physics*, Vol. 6 (Elsevier, 2013).